PNAS RESEARCH ARTICLE | NEUROSCIENCE

# Cross-regional coordination of activity in the human brain during autobiographical self-referential processing

James R. Stieger[a,b], Pedro Pinheiro-Chagas[a], Ying Fang[c], Jian Li[d], Zoe Lusk[a,b], Claire M. Perry[a,b], Manesh Girn[e], Diego Contreras[f], Qi Chen[c], John R. Huguenard[b,g], R. Nathan Spreng[e], Brian L. Edlow[d], Anthony D. Wagner[g,h], Vivek Buch[i], and Josef Parvizi[a,b,g,i,1]

Edited by Elizabeth Buffalo, University of Washington School of Medicine, Seattle, WA; received September 15, 2023; accepted June 10, 2024

**For the human brain to operate, populations of neurons across anatomical structures must coordinate their activity within milliseconds. To date, our understanding of such interactions has remained limited. We recorded directly from the hippocampus (HPC), posteromedial cortex (PMC), ventromedial/orbital prefrontal cortex (OFC), and the anterior nuclei of the thalamus (ANT) during two experiments of autobiographical memory processing that are known from decades of neuroimaging work to coactivate these regions. In 31 patients implanted with intracranial electrodes, we found that the presentation of memory retrieval cues elicited a significant increase of low frequency (LF < 6 Hz) activity followed by cross-regional phase coherence of this LF activity before select populations of neurons within each of the four regions increased high-frequency (HF > 70 Hz) activity. The power of HF activity was modulated by memory content, and its onset followed a specific temporal order of ANT→HPC/PMC→OFC. Further, we probed cross-regional causal effective interactions with repeated electrical pulses and found that HPC stimulations cause the greatest increase in LF-phase coherence across all regions, whereas the stimulation of any region caused the greatest LF-phase coherence between that particular region and ANT. These observations support the role of the ANT in gating, and the HPC in synchronizing, the activity of cortical midline structures when humans retrieve self-relevant memories of their past. Our findings offer a fresh perspective, with high temporal fidelity, about the dynamic signaling and underlying causal connections among distant regions when the brain is actively involved in retrieving self-referential memories from the past.**

default mode network | intracranial EEG | electrical stimulation | autobiographical | limbic network

## Significance

We recorded simultaneously from the human thalamus, hippocampus, posteromedial cortex, and orbitofrontal cortex during two autobiographical memory experiments and mapped their profile of activity and connectivity with millisecond resolution. Our findings provide significant insight into fast spatiotemporal dynamics of activity across distant structures of the brain as individuals are engaged in self-referential memory processing.

Neuroimaging studies have consistently and reliably identified several resting-state networks based on the slow dynamics (>1 s temporal windows) of cross-regionally correlated brain activity (1). Notably, diverse methods have substantiated the existence of these networks including the temporally synchronized slow (<1 Hz) modulation of higher frequency activity of intracranial electroencephalography (iEEG) across multiple sites within the same resting-state network (2–7) and direct recordings in mammalian brains that display laminar specificity and a temporal hierarchy of such ultraslow activity across remote brain regions (8).

While studying resting-state networks with functional magnetic resonance imaging (fMRI) provides valuable insights into the functional architecture of the human brain, examining the fast interactions and causal (effective) connections among nodes of the same functional network remains limited, if not prohibitive. In the current study, we aimed to extend the prior neuroimaging work by studying the dynamics of cross-regional communication in the subsecond (<1 s) scale. We conducted simultaneous intracranial recordings across nodes posited to belong to a well-known resting-state network, i.e., default mode network (DMN), and utilized repeated single electrical pulse stimulations in one site while recording the effect of such stimulations on all other sites—thereby measuring and quantifying the causal effective connectivity across the four regions. Simultaneous recordings across spatially distributed brain regions provide a precise lens on human circuit-level dynamics at the level of discrete neuronal populations while stimulation measures provide unique causal information in humans regarding the effect of stimulating one neuronal population on the activity of other sites as the dynamics of relationship between that site and others.

To examine the cross-regional interactions among disparate nodes of the brain during autobiographical memory processing, we recruited neurosurgical patients implanted with stereo-EEG electrodes (9) in the medial temporal, medial parietal, and ventromedial and orbital prefrontal cortical regions as part of the standard of care (10). In addition, some cortical electrodes were extended to reach the anterior nuclei of the thalamus (ANT) which provided a unique opportunity to study interactions between these structures and the canonical nodes of the DMN. Participating patients completed two complimentary autobiographical memory retrieval experiments (Fig. 1). We chose these four regions of the brain because of their debated anatomical location within the boundaries of DMN,

Author affiliations: [a]Laboratory of Behavioral and Cognitive Neuroscience, Human Intracranial Cognitive Electrophysiology Program, Stanford University School of Medicine, Stanford, CA 94305; [b]Department of Neurology and Neurological Sciences, Stanford School of Medicine, Stanford, CA 94305; [c]School of Psychology, South China Normal University, Guangzhou 510631, China; [d]Athinoula A. Martinos Center for Biomedical Imaging, Massachusetts General Hospital and Harvard Medical School, Charlestown, MA 02129; [e]Montreal Neurological Institute, Department Neurology and Neurosurgery, McGill University, Montreal, QC H3G 1A4, Canada; [f]Department of Neuroscience, University of Pennsylvania, School of Medicine, Philadelphia, PA 19104; [g]Wu Tsai Neurosciences Institute, Stanford, CA 94305; [h]Department of Psychology, Stanford University, Stanford, CA 94305; and [i]Department of Neurosurgery, Stanford University, Stanford School of Medicine, Stanford, CA 94305

Author contributions: J.P. and J.R.S. designed research; J.R.S., Z.L., C.M.P., V.B., and J.P. performed research; J.R.S., J.L., and M.G. contributed new analytic tools; J.R.S. analyzed electrophysiology data, J.L., B.E., M.G., and R.N.S. analyzed imaging data; and J.R.S. and J.P. wrote the paper. All authors contributed significantly in interpreting the data and editing the manuscript content.

The authors declare no competing interest.

This article is a PNAS Direct Submission.



[1]To whom correspondence may be addressed. Email: jparvizi@stanford.edu.

This article contains supporting information online at https://www.pnas.org/lookup/suppl/doi:10.1073/pnas.2316021121/-/DCSupplemental.

Published July 30, 2024.

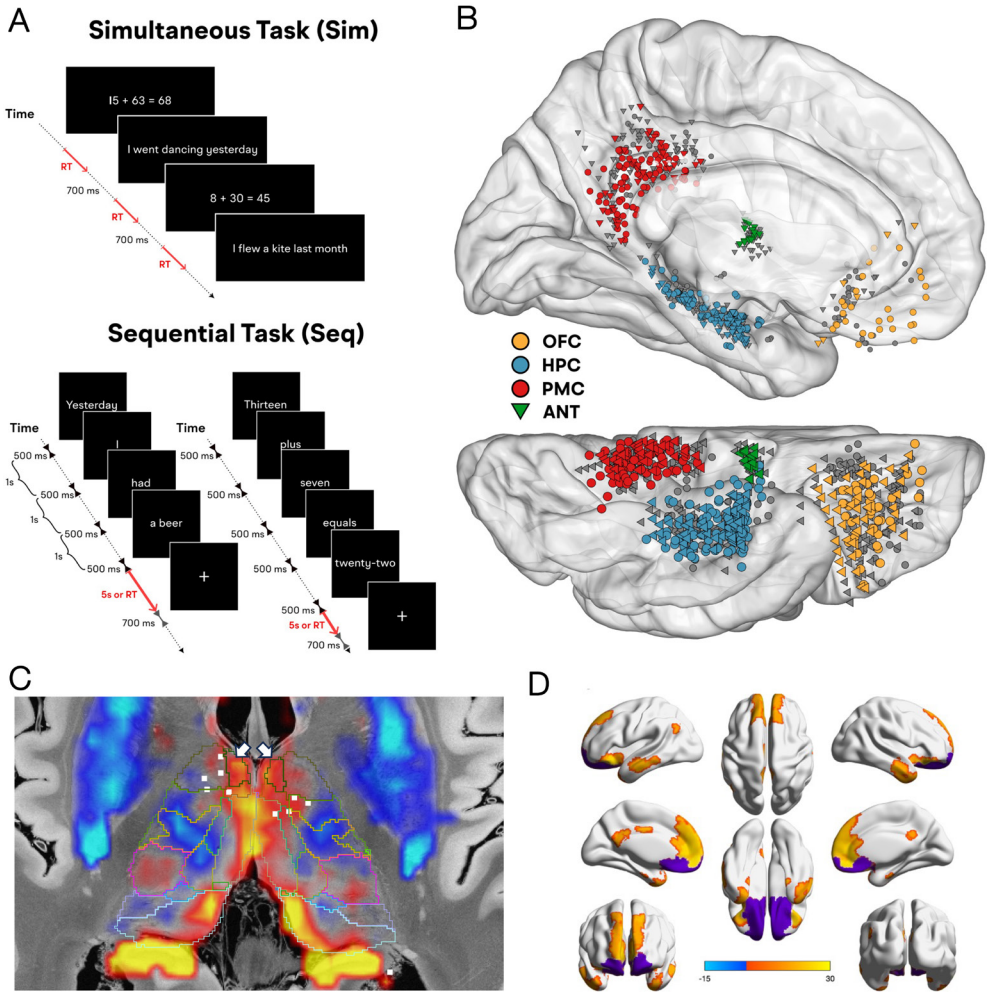


**Fig. 1.** Experimental tasks and regions. (*A*) Task design. Participants completed two tasks in which they decided whether a statement presented on the screen was true or false. The statements appeared in their entirety during the Sim Task (*A-Upper* panel) or presented one word at a time during the Seq Task (*A-Lower* panel). Note that a complete AM probe and non-AM probe in the Seq Task unfolded across 4 and 5 screens, respectively. Non-AM conditions in the Sim Task were either Math (in digit form only) or non-AM semantic statements (FACTS). Non-AM trials in the Seq Task contained Math statements appearing in both number-word (presented) and digit form. (*B*) Regions: We recruited 31 participants with 812 electrodes across four regions—OFC (n = 298), HPC (n = 248), PMC (n = 215), and anterior nuclei of the thalamus (ANT, n = 51; note: ANT recorded in a subset of 14 patients; covered sites in these participants are identified with triangles). Colored markers represent sites that displayed significantly increased HF power above baseline and during AM compared to non-AM trials in at least one of the tasks. OFC electrodes were located either in the vmPFC or orbital region of the PFC. All vmPFC electrodes were below the callosal level in the individual brain, but when projected from native space to standard space, some of these electrodes may appear to fall dorsal to this level. Relatedly, for visualization purposes, the HPC electrodes are projected to the surface, and some may appear out of the HPC in the standard space. All HPC electrodes were confirmed to be within the HPC in the native brain space. (*C*) Electrodes were mapped to the MNI space and overlaid with the subcortical maps of the DMN as described in Li et al. (19) (see *SI Appendix, Supplementary Material* for details). Note the location of electrodes compared to the ANT (arrows). (*D*) OFC seed region (purple) connectivity with 1,000 cortical parcels, thresholded at 90% sparsity (all values exceed Bonferroni $P < 0.01$ correction), reveals extensive connectivity with medial PFC, medial temporal lobes, PMC, and other regions part of the DMN. Resting-state functional connectivity from multiecho fMRI with TE-dependent denoising, as described by Girn et al. (20) (see *SI Appendix, Supplementary Material* for details).

and we focused on autobiographical memory condition, as the experimental task of interest, since decades of imaging and lesion studies have consistently documented the engagement and importance of these structures during autobiographical memory processing (11–18).

Our experiments were designed to address the following two fundamental questions currently unanswered in the field of memory research. First, what is the temporal sequence of events across the nodes of the network when individuals are engaged in retrieving self-referential memories. While decades of neuroimaging literature have confirmed the existence of a network of brain structures involved in this cognitive process (i.e., the default network), we seek to understand how each node of this network becomes activated with millisecond temporal resolution when individuals are retrieving such information. Second, can the temporal sequence of events identified in the correlative iEEG recordings be replicated with causal measures of intracranial electrical stimulation (iES)? To address this question, we will inquire about the extent of influence and the directionality of such influence across populations of neurons within this network. We discreetly identify the site of memory-related activations of neuronal populations in each of the four regions of interest during the memory retrieval condition and aim to replicate the temporal sequence of their activation using causal electrical stimulation. We explore the impact on other network nodes if a specific node is repeatedly stimulated with single pulses of electricity. Does the causal relationship across the four regions of interest exhibit symmetry, or do we observe asymmetric causality? While examining the time lags at the individual level could provide meaningful insights into the processing dynamics of pivotal nodes contributing to the memory system, examining the causal effect of stimulations in one node of the network on the other nodes of the network could provide unique, and hitherto largely missing, causal information that could guide the current theoretical models of memory processing.

## Results

**Demographics.** Our cohort consisted of 31 subjects with focal refractory epilepsy (*SI Appendix*, Table S1). All patients were undergoing invasive intracranial monitoring with stereoencephalography (sEEG) electrodes (AdTech Inc.) as part of routine clinical evaluations. While clinicians probed the source of seizure activity in these patients' brains, we invited them to participate in experiments during which they judged the accuracy of autobiographical episodic statements by retrieving memories of their past experiences (Fig. 1*A*, detailed in *Methods*) or rested quietly in their bed while electrical stimulation procedures were applied. The research protocol was approved by the Stanford University Institutional Review Board, and all subjects provided informed consent.

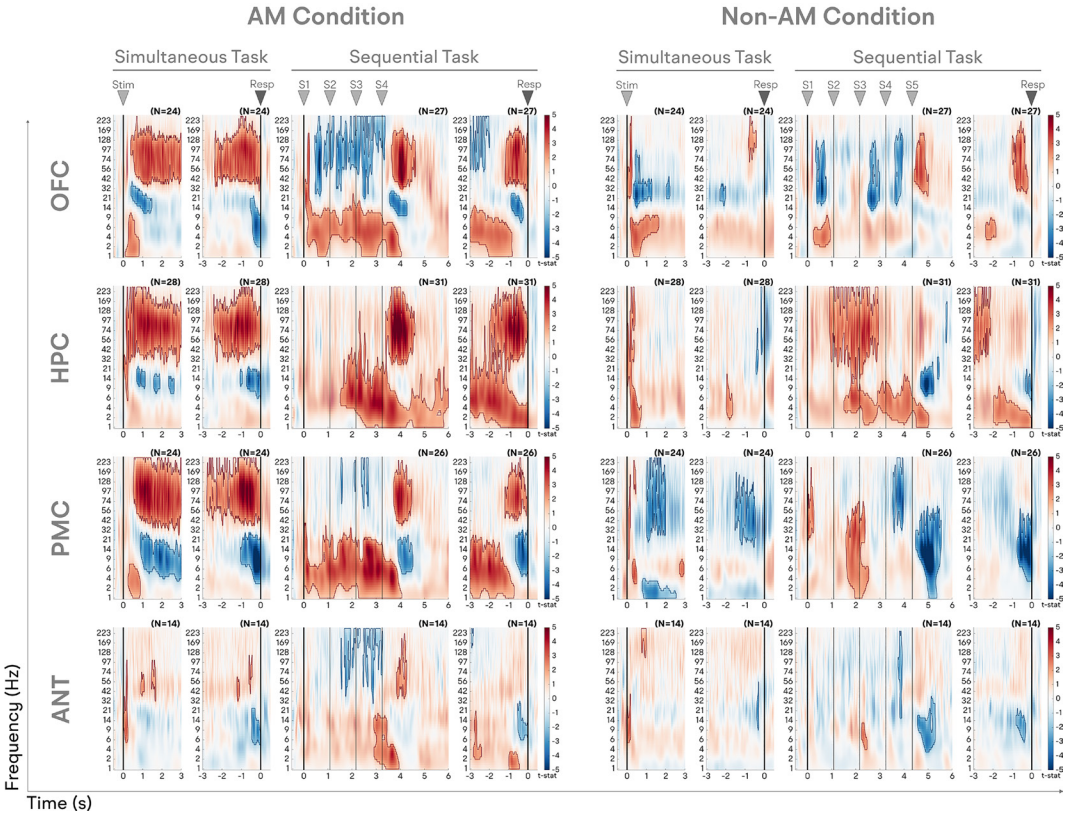


**Fig. 2.** Similarities and differences in the profile of activity across the four regions of interest. Each panel displays the group-level stimulus (Stim or S1-5) and response (Resp)-locked changes in power from baseline (prior to the presentation of the first stimulus) during the Sim and Seq Tasks. Note that the number of AM and non-AM stimuli in the Sim Task were 4 and 5, respectively (Fig. 1). (*Left*) Autobiographical memory processing (AM condition). (*Right*) Arithmetic calculation (non-AM/control condition). Vertical black lines in the sequential stim-locked panels show the time each stimulus was displayed (S1-5). The color represents the statistical reliability of increases (red) or decreases (blue) in power from baseline computed across patients with coverage in a given region (t-value against the null hypothesis of no change in power from baseline; the number of participants is presented above each panel). Significant deviations in power from baseline were identified with CBPTs. Significant time–frequency clusters are highlighted and outlined in red and blue (all $P < 0.0125$, Bonferroni corrected for four regions).

**Electrode Coverage.** We aggregated data from 812 recording sites across the left (N = 447) and right (N = 365) hemispheres and 4 ROIs: OFC [(total: per subject average ± SD) 298: 9.61 ± 6.47], HPC [248: 8.00 ± 3.94], posteromedial cortex (PMC) [215: 6.94 ± 5.73], and ANT [51: 1.65 ± 2.04]. It should be noted that only 14 patients had recordings in the thalamus (Fig. 1*B*). Twenty-six participants had implantation across at least three regions (i.e., ANT, HPC, PMC, or OFC) yielding sufficient data for within-subject and within-hemisphere analyses. The clinical rationale for thalamic recordings is detailed in our recent publication (21).

In this study, we simultaneously recorded from the human thalamus, as well as the hippocampus (HPC), the orbitofrontal cortex (OFC), and the medial parietal cortex in 31 subjects, involving 800+ recording sites, while the participants were engaged in two complimentary autobiographical memory retrieval experiments. We chose these four regions of the brain because decades of imaging and lesion studies have already documented their engagement during autobiographical memory processing.

**Behavioral Data.** Participants completed 268 ± 123 (AVG ± SD) trials in the Simultaneous Presentation (Sim) Task: 97 Autobiographical Memory (AM) and 97 non-AM (Fig. 1*A*) as well as Fact and Rest trials (i.e., a cross-hair appearing at the center of the screen when subjects were instructed to rest). These trials were excluded from the analysis. In the Sequential Presentation (Seq) Task, 220 ± 81 trials were completed (110 AM, 110 non-AM; Fig. 1*A*). The AM trials asked patients to judge the accuracy of common past experiences enabling their use with all participants (e.g., "Today I saw a doctor" or "Yesterday I took a shower"). The correct answer for the doctor and shower statement should be "Yes" and "No," respectively, because of the participant's surgery. We found that the subjects' responses were highly accurate for verifiable trials [Sim Task: subjects' accuracy = 91% ± 8%; Seq Task = subjects' accuracy= 83% ± 7%]. Likewise, the high level of participants' task engagement and the accuracy of their responses were documented by their high response accuracy during the non-AM (math) trials [Sim Task: 92.7% ± 6.1%; Sim Task: 89.5% ± 7.8%].

These findings confirmed that the participants understood the task requirements and remained engaged throughout the experiments (more details in *SI Appendix*, Table S2).

**Similarities and Differences in Power Spectral Patterns across Regions.** We included recorded signals from every available site within every region to assess the similarities and differences in power spectral patterns across all four regions during the AM condition (Fig. 2—"AM-Condition"). In the Sim Task, AM-related sites in the HPC, PMC, and OFC responded with an initial, transient significant increase in the power of low-frequency activity (LF; 1 to 6 Hz) followed by a decrease in mid-range frequencies (~8 to 30 Hz, overlapping with the traditional alpha and beta ranges) and increase in high-gamma (70 to 170 Hz) power—akin to prior observations during other cognitive tasks (22–24). Of note, 62% of ANT sites displayed greater power in gamma (32 to 58 Hz) than high-gamma range [$T(50) = 2.24$, $P = 0.029$]. For simplicity, we refer to high-gamma activity in the HPC, PMC, and OFC and gamma activity in the ANT as "high-frequency, HF" activity and power changes in the low frequencies of the field as "low-frequency, LF" activity. In the AM condition of the Seq Task, when the presentation of each stimulus was timed and sequential, a significant increase in the HF range occurred in all regions after the last stimulus [Mixed-Effects Models (MxM): $F(775) = 14.43$, $P < 0.0001$]. By comparison, LF activity in all regions was locked to the presentation of each stimulus (Fig. 2). Mixed effects models (MxM) confirmed that this effect was stronger during AM than non-AM trials [*SI Appendix*, Tables S3 and S4; LF memory effect (MxM): $F(567) = 7.39$, $P = 0.0007$, HF memory effect (MxM): $F(684) = 10.31$, $P < 0.0001$—unless

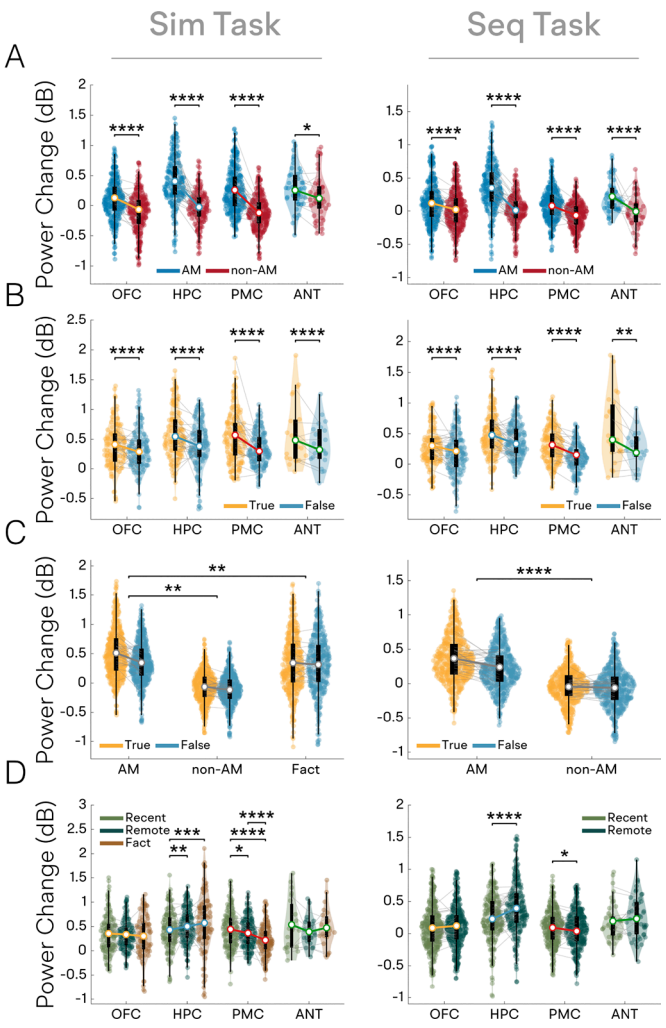


**Fig. 3.** HF power (70 to 170 Hz) in each region is modulated by the memory content. Dissociable effects of memory content are shown for (*A*) task condition; (*B* and *C*) subject's true or false responses to memory statements; and (*D*) memory age. (*A*) All ROIs in our study displayed greater increases in HF power for AM compared to non-AM trials (all $P < 0.01$). (*B*) In all ROIs, greater power of HF activity was recorded during AM trials that were rated by the subject as "True" compared to "False" ($P < 0.004$). (*C*) This increased HF power for "True" subject ratings was specific to the AM condition, displaying a greater difference between HF power for "True" vs. "False" ratings in AM trials than both non-AM (math; $P < 0.003$) and fact ($P = 0.007$) trials. (*D*) While the HPC produced greater HF power for remote compared to recent memories ($P < 0.002$)—the reverse pattern was seen across PMC electrodes where a greater HF power was captured during retrieval of recent compared to remote memories ($P < 0.04$). In the violin plots, each colored dot represents one electrode, black boxes display the interquartile range, gray lines show individual subject averages, and colored lines show the average across subjects. (*$P$ <= 0.05, **$P$ <= 0.01, ***$P$ <= 0.001, and ****$P$ < 0.0001, corrected for multiple comparisons). (See *SI Appendix*, Tables S3–S5 for full Statistics). See *Methods* for definition of each memory content type.

otherwise noted, results reported in the text apply to both tasks, but statistics are reported only for the Sim Task to reduce repetition]. These findings demonstrate that the average of recorded signals for every region (including all sites without selection bias) displayed a similar profile of power spectral pattern in the AM condition.

**Proportion of Recording Sites Displaying Significant Responses during AM Processing.** We then identified the recording sites that displayed higher activation—as indexed by the power of HF activity during AM trials compared to both baseline (i.e., a subset of the 700 ms intertrial interval) and the non-AM (Math) condition. We emphasize that the rationale for choosing both the baseline and the non-AM condition was not to claim selectivity but to exclude responses linked to motor (e.g., clicking mouse button) or to generic attention or visual processing. In the Sim Task, subjects also evaluated semantic statements labeled as Facts (e.g., "Paris is in Europe"). These trials served as another non-AM control condition. Our analysis identified different proportions of sites per region that were more significantly engaged during the AM condition, with the highest proportion noted in the HPC (56% ± 33%) followed by the PMC (54% ± 34%), OFC (37% ± 28%), and ANT (21% ± 37%) (colored sites in Fig. 1*B*). These findings demonstrate that in a given region, only select populations of neurons are engaged during the studied cognitive process.

**Modulation of HF Activity by Memory Content.** It is well established in the field of autobiographical memory research that participants (when making judgments about autobiographical statements) are engaged in a myriad of cognitive processes such as episodic retrieval, self-reflection, emotion, and semantic reasoning (25). To examine whether the recorded HF activity was related to memory processing, rather than generic decision-making or response preparation processes, we measured the effect of the semantic content of memory statements on the power of induced neural activity. To avoid bias in selecting a specific temporal window for power analysis, we chose stim-locked (500 to 1,500 ms following the retrieval cue) as well as response-locked (1 s prior to response) windows and compared the HF power as a function of memory content. These comparisons represent changes in HF power from the pretrial baseline of 500 to 200 ms before the first stimulus. We analyzed HF power across different conditions of memory age ("remote" such as "Last month" vs. "recent" such as "Today" etc.) and subject's response (responded as "True" i.e., correct hits vs. responded as "False" i.e., correct rejections) (Fig. 3 and *SI Appendix*, Table S4 for statistical details).

Across all four regions, correct hits elicited significantly more HF activity than correct rejections [patient response—(MxM): $F(705) = 12.33$, $P = 0.0005$, True–False: $T(705) = 8.05$, $P < 0.0001$]. Moreover, this effect was specific to the AM condition. In both tasks, we found the True–False HF power contrast was significantly greater in AM trials compared to math trials [(MxM): $T(1698) = 3.03$, $P = 0.003$]. We also found this contrast to be significantly greater than the fact trials [(MxM): $T(1698) = 3.39$, $P = 0.007$], which did not display a significant difference between true and false responses [(MxM): $T(1698) = 1.07$, $P = 0.28$]. The same effects of patient response were seen in the verifiably "True" and "False" responses [(MxM): $F(713) = 28.45$, $P < 0.0001$]. These results suggest the increased HF power observed within the ROIs in our study is specific to the AM process with greater HF power increases observed when subjects rate an AM statement as true. However, we also observed an interaction between memory content and HF power suggesting regional HF activity was not homogenous across all regions. For instance, consistent with a recent study of hippocampal sharp ripples (26), the HPC recording sites showed stronger HF activity during the processing of remote vs. recent memories [memory age—(MxM): $F(1276) = 4.11$, $P = 0.0004$, HPC recent-remote: –0.12dB $T(1260) = -3.48$, $P = 0.0015$] but the opposite was the case in the PMC [PMC recent-remote: +0.08dB $T(1280) = 2.66$, $P = 0.02$]. ANT sites revealed higher HF power for AM trials [+0.17dB $T(684) = 2.50$, $P = 0.01$] and "True" trials [+0.15dB $T(705) = 8.05$, $P < 0.0001$], but no effect for memory age [+0.06dB $T(1260) = 0.75$, $P = 0.74$] (*SI Appendix*, Fig. S1*C* and Table S5).

We additionally analyzed hippocampal sharp wave ripples (SWR) in order to see how similar our results would be between SWRs and HF activity (26). We found that the average ripple rate and change in HF power across the AM and non-AM conditions were significantly correlated across the AM-related sites [Sim: $r(138) = 0.69$, $P < 0.0001$,

Seq: r(155) = 0.53, $P < 0.0001$], but not unrelated sites [Sim r(52) = 0.08, $P = 0.41$, Seq r(69) = 0.05, $P = 0.52$]. Broadly speaking, we see the same effects in the SWR analysis as the HF power analysis such as an increase in ripple rate for the AM compared to the non-AM condition [(MxM): T(331) = 8.26, $P < 0.0001$], for "True" responses compared to "False" responses [(MxM): T(180) = 6.69, $P < 0.0001$], and remote compared to recent trials [Seq: (MxM): T(219) = 7.21, $P < 0.0001$]. Importantly, in the Sim Task, we see a significant gradient of increasing ripple rate from recent to remote trials [(MxM): T(312) = 5.08, $P < 0.0001$] and from remote to fact trials [(MxM): T(315) = 4.13, $P = 0.0001$]. The differences in significant effects between HF power and ripple rate could be due to the greater specificity of the SWR analysis.

These findings demonstrate that the recorded electrophysiological responses tracked the behavior of the participants. The consistency of these effects observed across both tasks suggests the following: 1) our findings can be attributable to the AM process rather than a confound of task design, and 2) while the regions predominantly display similar activity, each region's role in AM processing is at least partially distinct because the modulation of activity by memory content is not homogenous across sites.

**Cross-Regional Phase Coherence Following the Retrieval Cue.** To explore how oscillations across regions are coordinated and synchronized, we measured phase coherence, which reflects the degree to which the phase of signals in two brain regions—that are themselves formed as a result of the summation of postsynaptic potentials generated in a large number of neurons (27)—are coherent. For this, we measured 1) regional phase coherence across all trials in a given region (labeled as intertrial-phase coherence, ITPC; *SI Appendix*, Fig. S2), 2) phase coherence in a given region across the two hemispheres (labeled as interhemispheric within-region phase coherence, $ISPC_{within}$; *SI Appendix*, Fig. S3), and 3) phase coherence between two different regions (labeled as between region intersite phase coherence, $ISPC_{between}$; *SI Appendix*, Figs. S4 and S5). We confirmed the presence of oscillations in the power spectrum in the form of peaks in the LF range above the aperiodic background utilizing a method as described elsewhere (28). Additional post hoc tests verified these results were not driven by volume conduction or choice of common average referencing (*SI Appendix*, *Supplementary Material*).

A significant ITPC was found in all regions in the LF range following the appearance of each stimulus. This effect was observed during both AM and non-AM trials in both Simultaneous and Seq Tasks [cluster-based permutation tests (CBPT); $P < 0.003$]. The contrast between ITPC findings and ISPC findings was most clear during Seq Task: Unlike significant increases in ITPC after each stimulus, we observed increased ISPC only after the final stimulus was presented. This last stimulus was the associative memory cue that prompted the participant to begin making memory-based decisions in AM and Math conditions [CBPT; $P < 0.002$]. Of note, in the non-AM (Math) condition, the increase in cross-regional coherence did not occur when the subjects were adding numbers together, but rather when the number on the screen was being compared to the calculated value stored in memory. We additionally measured ISPC across time and found that when the ANT and PMC cohere with the HPC in the LF range, both display greater ISPC during AM vs. math conditions [(MxM): Zr>4.77, $P < 0.0001$] and that the AM-related sites show greater ISPC than the non-AM sites [(MxM): Zr>4.77, $P < 0.0001$].

The above findings demonstrate that consistent phase relations within regions occur nonselectively after the presentation of each stimulus regardless of its content, while the phase relations between sites are selective to the time when participants were engaged in retrieving memory-based information. We are confident that the ITPC findings were not simply due to visual evoked potentials since the plotted raw EEG signals during both AM and non-AM conditions did not show similar time-locked changes after each visual stimulus (*SI Appendix*, Fig. S6). However, the ITPC and even ISPC findings could be related to the phenomenon of "cognitive" event-related potentials (ERPs) that have been hypothesized to be caused by stimulus-induced increases in the phase-locking of ongoing EEG activity (29, 30) but not visually evoked changes in the EEG power alone (31).

**Timing of Hippocampal LF Power and Cross-Regional Phase Coherence.** By leveraging the high temporal resolution of our approach, we used a measure of response onset latency (ROL, detailed in *SI Appendix*, Fig. S7 and *Supplementary Materials*) to explore how changes in the power of LF or HF activity and the coupling of phase between remote sites ($ISPC_{between}$) relate to each other across time. We specifically examined whether these features occur simultaneously or progress in stages while the participants engaged in autobiographical processing (Fig. 4). To compare the timing of events across sites, we only used data across pairs of sites within the same hemisphere and within the same subject. This analysis revealed a specific temporal order of rising LF power in all regions, followed by coupling between sites ($ISPC_{between}$; hereafter referred to as ISPC) and finally rising HF power. Interestingly, the same statistical pattern was seen during the AM condition in both experimental tasks [(MxM): F(1026) = 12.73, $P < 0.0001$; see *SI Appendix*, Tables S6–S8 for detailed stats].

The timing of LF activity in the HPC and ANT was more noteworthy in that it persisted longer and was present when the LF activity in the OFC and PMC had already subsided [Fig. 4 *B*, *Left*, MxM: T(964) > 2.77, $P < 0.029$; see *SI Appendix*, Tables S6 and S7]. However, the nature of the LF power differed between the HPC and ANT. In the HPC, the probability density function (PDF) of LF activity peaked after the recall cue and persisted along with the ISPC PDF, while the probability of ANT LF activity (like OFC and PMC) dropped sharply before the peak of the ISPC PDF but displayed a higher probability near the end of the trial.

In terms of the timing of HF activity, the ANT HF power appeared first while the OFC HF power appeared last [Early ANT HF—(MxM): ANT-HPC/OFC: T(1029) < −2.63, $P < 0.04$; ANT-PMC was only significant in the Sim Task: T(963) = 4.93, $P < 0.0001$; Late OFC HF—(MxM): OFC-Others: T(1034) > 5.65, $P < 0.0001$]. The time of HF activity in the HPC and PMC did not differ [Fig. 4 *B*, *Right*, (MxM): T(1031) = 0.86, $P = 0.83$]. As seen in Fig. 4*C*, these data highlight three important findings: First, the onset of HPC LF activity is contemporaneous with the global LF synchronization (ISPC); second, the HF activity in the ANT is the first to erupt before the HF activity in other regions is triggered; and third, the OFC is the last region in this HF cascade.

***Probing cross-regional interplay with causal measures.*** To provide causal information, we applied electrical stimulation using the well-known method of single-pulse electrical stimulation (SPES; referred to as STIM for ease of understanding). In this procedure, repeated single pulses were delivered, during the resting state, between adjacent pairs of implanted electrodes while recording from all other implanted electrodes in an individual subject's brain (32). The presence and timing of evoked responses in a recorded region suggests that the stimulated seed region is physiologically connected with, and has the means to exert an effect upon, the target site (33–35). While these analyses are not directly linked to AM processing, they provide important information concerning the causal information flow between regions, which may guide future models of the mechanisms of cross-regional electrophysiological interactions within the purported nodes of the DMN.

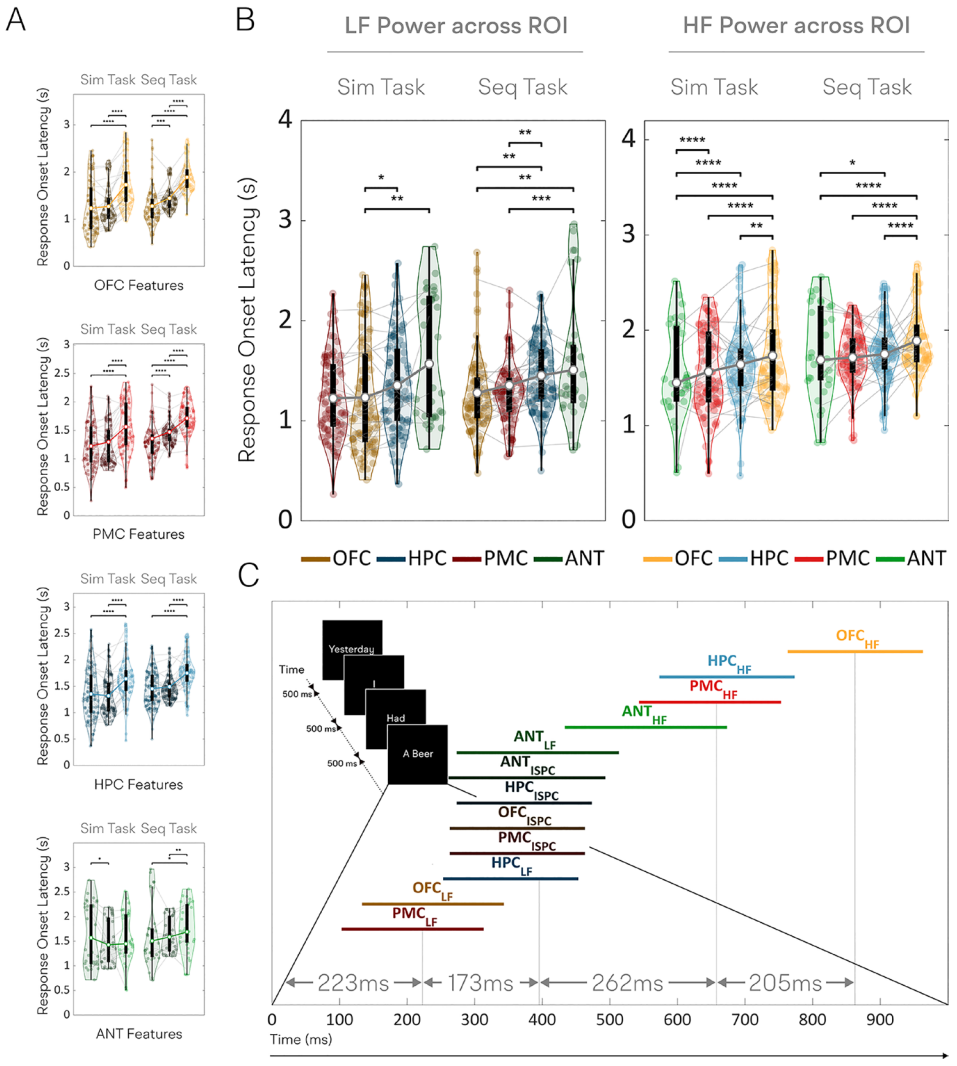


**Fig. 4.** Temporal profiles of electrophysiological activity during autobiographical memory processing. (*A*) ROL estimates for individual electrodes in each region for LF power, ISPC, and HF power (in that order) during Simultaneous and Seq Tasks. An interesting temporal order was seen when modeling ROL ($P < 0.0001$). (*B*) ROL of LF (*Left*) and HF (*Right*) power compared across regions. Violin plots: Each colored dot represents the ROL of one feature within a given electrode, black boxes display the interquartile range, gray lines show individual subject averages, and colored lines show the average across subjects. (****$P <= 0.0001$). (*C*) The *Lower* panel shows the 95% CI for the estimates of each region feature following the final stimulus in the Seq Task. The vertical lines represent significant differences between groups of features. Note: Results come from sites with significant AM-related activations identified in Fig. 1*B* (all ANT electrodes were included and reflect the ROL of gamma power).

Using data from the STIM approach, we collected descriptive data regarding the extent of causal effective connectivity across the four regions. We found a large proportion of stimulated sites within the HPC causing significant time-locked evoked responses in the ANT (74.2% ± 6.5%), PMC (51.2% ± 10.2%), and OFC (36.2% ± 7.1%). However, the proportion of sites in each of the other regions whose stimulation generated evoked responses in the HPC was smaller (details in Fig. 5*A* and *SI Appendix*, Table S9). The ANT, on the other hand, appeared to have bidirectional effective connectivity with the OFC (in the following, X→Y means stimulate X, record in Y: ANT→OFC: 56.8% ± 10.2%; OFC→ANT: 58.3% ± 12.2%) and PMC (ANT→PMC: 41.3% ± 10.6%; PMC→ANT: 33.5% ± 6.2%), suggesting that the ANT is strongly influenced by incoming signals from the HPC while it bidirectionally communicates with the OFC and PMC.

The descriptive data, presented above, only reflect the extent of connectivity (i.e., the proportion of sites within a region influencing sites in another region). In a separate analysis, we quantified the robustness of connections between a pair of sites using the measure of "Connectivity Index" (*SI Appendix*, Fig. S9 and *Supplementary Material*). This measure is based on the prediction that if A→B connections are robust, then stimulations in A will reliably evoke coherent responses in B (across multiple trials of stimulation), whereas if the connections are less robust and noisy, the evoked responses will be closer to noise and less coherent.

Across all pairs of stimulated-recorded sites, we confirmed significantly greater measures of Connectivity Index across pairs of sites that happened to be coactivated during the AM condition [(MxM): $F(2563) = 2.10$, $P = 0.002$; Act→Act>Non-Act: $Zr = 3.22$, $P = 0.001$ *SI Appendix*, Table S10]. However, the strength of connectivity was not the same in both directions between regions [(MxM): $F(1064) = 50.11$, $P < 0.0001$] which suggests an asymmetric directionality of signal flow across different regions of the network (Fig. 5 *B*–*E*). For instance, the strength of connectivity from the HPC to all other regions was significantly stronger than from other regions to the HPC [outflow>inflow—(MxM): $Zr = 7.89$, $P < 0.0001$; red stars in Fig. 5 *A* and *E*—the size of arrows in Fig. 5*E* scales with Connectivity Index]. Therefore, the stimulation of the HPC changes the activity of other regions but the stimulation of the other three regions does not equally affect the HPC–although the HPC still receives some significant connections from those regions. By contrast, the ANT appears to receive the greatest proportion of evoked responses following the stimulation of any other region [inflow>outflow—(MxM): $Zr = 3.94$, $P = 0.0001$]. The ANT and HPC also appear to differentially affect cortex (Fig. 5*C*). While the HPC has a greater influence over the ANT than the cortex [CTX–OFC, PMC in Fig. 5 *C*, *Left*; (MxM): $Zr = 5.27$, $P < 0.0001$], the ANT has a greater influence over the cortex than the HPC [*Right*; (MxM): $Zr = 4.20$, $P < 0.0001$]. Finally, the ANT displays a selective affinity to the OFC (Fig. 5*D*). The influence of both ANT→OFC and OFC→ANT is stronger

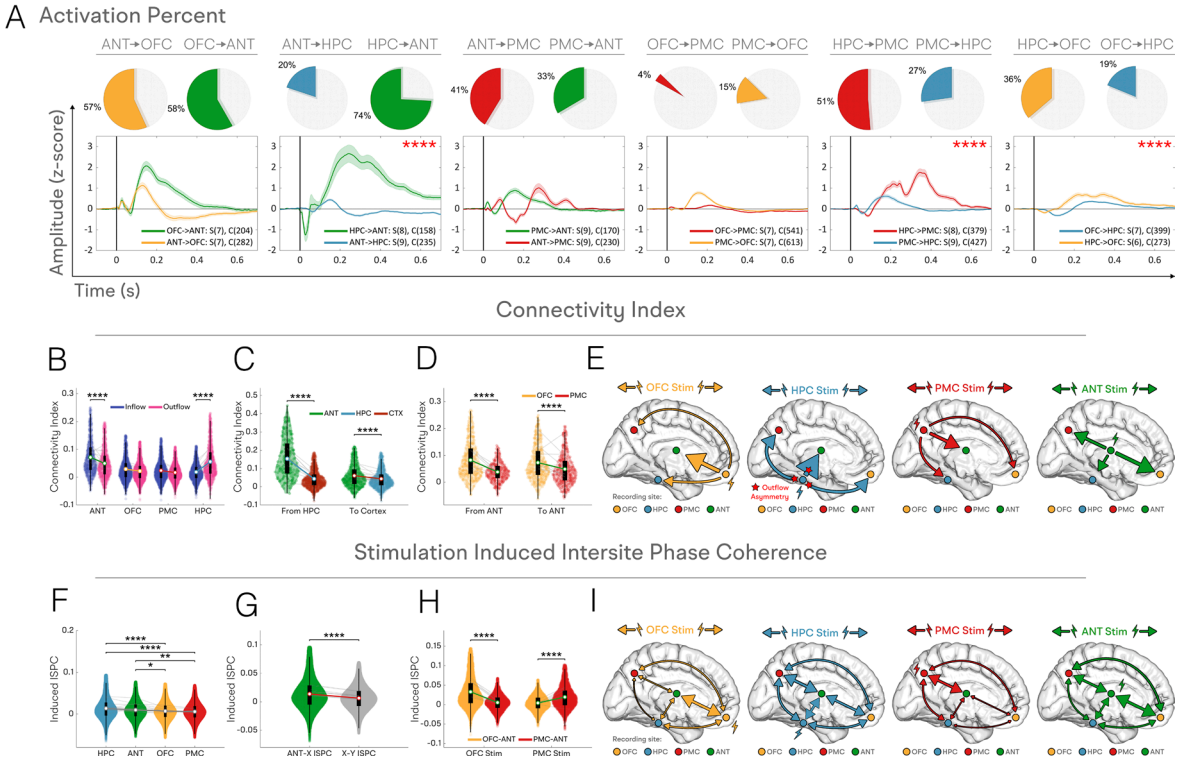


**Fig. 5.** Profile of effective connectivity across regions reveals a directionally asymmetric axis of influence between regions. (*A*) Causal effective connectivity with single pulse electrical stimulation. (*Upper*) Percentage of stimulation sites causing significant voltage deflections in recording sites within distant regions (X→Y: stimulate X, record in Y). (*Lower*) Each plot shows the average voltage deflection response of a given region to single pulses of electrical stimulation in another region (S: number of subjects; C: number of connection pairs). The red stars in the upper right of the panels indicate the HPC→X connectivity index is significantly greater than in the X→HPC direction. (*B–E*) A connectivity index based on intertrial phase coherence (ITPC) was derived as a measure of how consistently single pulses of electricity in one region affect the voltage in another region (*SI Appendix*, *Supplementary Material*, Fig. S9, and Statistics: Table S10). (*B*) Asymmetrical influence of inflow vs. outflow for the ANT and HPC. Inflow represents the connectivity index in response to stimulation (X→ROI: stimulate any X, record in ROI), outflow represents the converse (ROI→X: stimulate ROI, record in any X). The influence of the HPC on other regions was significantly greater than the influence of other regions on the HPC (all $P <= 0.0002$; red stars indicate significant directional effects in panels *A* and *E*). The ANT, however, displays significantly greater inflow than outflow ($P < 0.0001$). (*C*) The ANT and HPC have a differential relationship to the cortex. (*Left*) The HPC has a greater influence over the ANT than the cortex (CTX-OFC, PMC; $P < 0.0001$). (*Right*) The ANT has a greater influence on the cortex than the HPC ($P < 0.0001$). (*D*) The ANT displays a selective affinity to the OFC. The influence of both ANT→OFC and OFC→ANT is stronger than ANT's relationship with the PMC (both $P < 0.0001$). (*E*) Model of connectivity index between all ROI pairs. Arrows are drawn in proportion to the strength of the connectivity index from the stimulated site (labeled above plots with lightning bolts) to the site where ITPC was recorded (circles; recording ROIs labeled below plots). Red stars indicate HPC→X is significantly greater than X→HPC. (*F–I*) Stimulation-induced ISPC. A similar metric was derived to the connectivity index; however, in these plots, we measured the ISPC between all regional pairs in response to stimulation rather than the individual channel ITPC (*SI Appendix*, Statistics: Table S11). (*F*) HPC ($P < 0.0001$) and ANT ($P < 0.01$) stimulation leads to greater ISPC than cortex. Here, the stimulated site is on the x-axis and the violins represent the change in ISPC across all ROI pairs. (*G*) Following stimulation, ISPC was greater between ANT pairing with other ROIs (ROI→ANT-X: stimulate any ROI, record the ISPC between ANT and any other ROI X) than any other ROI pairs (ROI→X-Y: stimulate any ROI, record the ISPC between any two other ROIs X and Y; $P < 0.0001$). This effect is most clearly seen in panel (*H*) which documents ANT coherence with stimulated cortical sites. When the OFC is stimulated, the strongest observed ISPC is between the OFC and ANT which is significantly stronger than the ISPC between the PMC and ANT ($P < 0.0001$), but when the PMC is stimulated, the PMC displays the stronger ISPC with the ANT ($P < 0.0001$). (*I*) Model of induced ISPC between all ROI pairs. Arrows are drawn in proportion to the strength of induced ISPC between recording sites (circles; recording ROIs labeled below plots) in response to stimulation (labeled above plots with lightning bolts).

than ANT's relationship with PMC [OFC→ANT > PMC→ANT (MxM): Zr = 4.11, $P < 0.0001$; ANT→OFC > ANT→PMC (MxM): Zr = 5.03, $P < 0.0001$]. Importantly, we validated these findings by showing the thalamic recording sites closer to the ANT proper were more likely to display evoked responses following OFC stimulation [OFC→ANT vs. distance: r(24) = −0.46, $P = 0.041$], and vice versa [ANT→OFC vs. distance: r(24) = −0.52, $P = 0.027$; see *SI Appendix*, Fig. S1*F*].

The measure of stimulation-induced ISPC also affirmed the generalizations mentioned above (Fig. 5 *F–I* and *SI Appendix*, Table S11). In this analysis, we measured the increase in phase coherence between pairs of sites resulting from stimulating a given region. This is different than the measure of the Connectivity Index which relies on trial-by-trial coherence between responses within a single electrode as a result of stimulating another seed region (i.e., ITPC). Here, following stimulation of a seed region, we measured ISPC between all region pairs (after excluding contacts affected by the stimulation artifact). We found that the stimulation of the HPC and ANT, on average, produced more observed increases in ISPC across all electrode pairs than the OFC or PMC [in the following ROI→X-Y means stimulate ROI, record ISPC between any two ROIs X and Y: HPC→(X-Y ISPC) > OFC→(X-Y ISPC) (MxM): Zr = 4.71, $P < 0.0001$; HPC→ > PMC→ (MxM): Zr = 5.28, $P < 0.0001$; ANT→ > OFC→ (MxM): Zr = 3.08, $P = 0.01$; ANT→ > PMC→ (MxM): Zr = 3.59, $P = 0.002$]. In contrast, the stimulation of each region caused the greatest ISPC between that particular region and ANT [X→(X-ANT ISPC) > X→(Z-Y ISPC) (MxM): Zr = 20.72, $P < 0.0001$]. This highlights the importance of ANT's role as a universal receiver of information in that, following stimulation of any region, the ANT was most likely to synchronize its activity with the stimulated region (Fig. 5 *H* and *I*). This effect is most clearly seen for OFC and PMC stimulation, in that the stimulated site displays greater coherence with the ANT than the other cortical site, regardless of ANT affinity with the OFC [Fig. 5*H*; OFC→OFC-ANT > PMC-ANT (MxM): Zr = 30.59, $P < 0.0001$; PMC→PMC-ANT > OFC-ANT (MxM): Zr = 25.71, $P < 0.0001$]. These results are shown with arrows proportional to the stimulation-induced ISPC in Fig. 5*I* (further statistical

details found in *SI Appendix*, Table S11). ISPC measures were once again stronger between sites that were coengaged during the AM condition (i.e., increased HF activity compared to baseline and non-AM condition) than sites that were not [Act→Act>Non-Act—(MxM): Zr = 5.45, $P < 0.0001$].

Finally, we calculated the speed of signal flow across regions by measuring the time to the first prominent peak in sites displaying significant evoked responses (details *SI Appendix*, Table S12). These results highlighted the centrality of the ANT among the regions of interest studied here. For instance, the speed of connectivity from a region to the ANT was significantly faster than the speed of connections from the same ANT to the other regional sites [$T(44) = 3.43$, $P = 0.0026$]. Furthermore, connections from the ANT to the other regions (on average) were significantly faster than the connections among the other regions [$T(61) = 2.62$, $P = 0.01$].

The above findings demonstrate that only a select proportion of populations of neurons are connected across different regions and that the proportionality and strength of these connections are asymmetric. Further, we found more robust connections across pairs of populations that are coengaged during the experimental condition. More notably, the outward connections of the HPC to all regions stand in contrast to inward and fast connection of all regions toward the ANT.

## Discussion

In an attempt to understand the neurophysiological mode of cross-regional interactions in the human brain, we focused on the brain regions associated with the DMN as the network of our choice and autobiographical memory processing as the paragon experimental paradigm given the large body of lesion and imaging studies in the past decades showing strong coactivation of the DMN structures during this cognitive function (11–18).

**Main Contribution of Our Study.** The significant and innovative aspects of our work pertain to the i) use of a sequential memory task that offered greater temporal granularity, ii) simultaneous intracranial recordings across a broad range of cortical and subcortical regions—most notably the human thalamus—and iii) the combination of iEEG recordings and iES measures to causally investigate neural responses and circuit dynamics.

Our research presents unique electrophysiological evidence demonstrating that the retrieval of autobiographical memories entails a coordinated series of neural events unfolding in a specific temporal order across cortical and subcortical brain regions. Our study also contributes to the current wave of literature suggesting that the lower structures of the brain (i.e., subcortical structures such as the thalamus) contribute meaningfully to the processing of higher cognitive functions - beyond serving as a mere relay for other structures.

***Highlights of our correlative findings.*** We analyzed signals across all electrodes present within the boundaries of each region and observed that, within each region, only select populations of neurons were engaged during the experimental task (Fig. 1, colored vs. gray sites). Next, we observed a remarkably similar "signature" of electrophysiological activity across all four regions in the subsecond space (Fig. 2). The profile of HF and LF activity in the Sim Task was similar to the one obtained during the Seq Task—i.e., in the time window after the presentation of the memory cue—which offered a replication of our findings across two complementary tasks while providing important information about the time of coengagement across the four regions after the presentation of the memory cue. Further, we confirmed that the stimulus-locked (500 to 1,500 ms following the retrieval cue) as well as response-locked (1,000 ms prior to response) power of HF activity was higher in hit statements compared to correct rejections and modulated by the cognitive content of memory statements (i.e., remote vs. recent, true vs. false) suggesting that the observed electrophysiological features were not independent of the cognitive content of the stimuli (Fig. 3). In addition to differential activity documented across various memory contents following the retrieval cue, our findings also revealed differences in the mode of activity across regions during the stimuli preceding the presentation of the memory cue in the Seq Task. We interpret these regionally specific signatures of electrophysiological activity as preliminary evidence that the contribution of each region to different stages of memory retrieval may be unique and can be decoded in future studies employing more specific task designs.

The above observations are derived from data collected from all recording sites within each region. This may have diluted our results from the cortical sites because each region was defined solely based on anatomical boundaries. Thus, different recording sites within those boundaries may have represented different functional units. To better understand how functionally similar neuronal populations across the four regions interact with each other, and to compare the time of their engagement, we selected only AM-activated sites within each region and studied how their responses unfolded in time and interregional coupling. This analysis revealed a unique temporal order of events across frequencies (LF to HF) and across regions—a finding that was made possible because of simultaneous recordings with high temporal resolution and, more importantly, a high signal-to-noise ratio of observed physiological responses enabling within-subject and trial-by-trial comparisons. After the presentation of the memory cue in the Seq Task, when participants attempted to construct mental representations of cued personal past events, a cascade of temporally orchestrated electrophysiological events unfolded across the studied regions: regional LF activity → cross-regional phase coherence of LF activity → regional HF activity (*SI Appendix*, Figs. S2–S5). The spectral pattern of increased theta, decreased alpha, and increased gamma power during memory retrieval has also been documented in scalp EEG (36) Some interpret this altered pattern as a single process caused by the spectral tilt or change in the 1/f slope (28) The earlier rise in LF activity reported here could therefore be an artifact of low-frequency filtering. However, evidence from the Seq Task in Fig. 2 argues against this possibility. In the stimulus-locked plots, we observe significant increases in LF power throughout the entire trial. Then, when the HF power increase occurs, the LF power falls off in the OFC and PMC while it persists in the HPC. This is most clearly seen in the response-locked plots. If the LF activity was merely an artifact of the HF envelope rather than a distinct spectral representation of neural activity, we would expect to see the same pattern across ROIs. The temporal order of events documented here thus shows the temporal relationship between LF and HF activities in the brain as well as the sequence of activations in time across the four regions.

***Highlights of our causal findings.*** As temporal regularities do not necessarily imply causation (37), it was important for us to reproduce and confirm the main findings derived from our correlation-based approach using causal information obtained with the electrical stimulation approach. We emphasize, however, that the term "causal" here refers to the process of one event (evoked responses in recording sites) directly contributed to the occurrence of another event (repeated stimulation in another region), and does not necessarily imply that these events are necessary and or sufficient for memory processing per se. Our causal data are presented here to supplement or validate the

correlative data recorded with iEEG. As detailed in Fig. 5 and related supplementary material, our causal approach supported our correlative data in several ways. We found that i) the extent of causal effective connectivity between two regions was asymmetric (i.e., while many sites in a given region caused evoked responses in another region (A → B), only a small number of sites would do the same in return (B → A). ii) causal connectivity between a pair of recording sites, across two regions, was stronger if the two sites were coactivated during the experimental AM-condition; iii) stimulation of the HPC, on average, produced the greatest observed outflow effect on other ROIs; while iv) the ANT displayed the greatest inflow effect.

**DMN and Autobiographical Memory Retrieval.** During autobiographical memory retrieval, a reconstructive process is thought to be ignited in which the retrieval of episodic details (those that are still accessible) is mixed with imagination, inferential reasoning, as well as emotional processing (38, 39). While our study was not specifically designed to unravel the precise role of each brain region in such a complex set of functions, the profile of activity of each of the four regions may provide clues about their contribution to the process of autobiographical retrieval.

***HPC–PMC axis of engagement during autobiographical memory retrieval.*** The hippocampus's role in the retrieval of (specially older) episodic memories has been a subject of debate since early studies of patient HM led to a belief that the HPC may not be necessary for such functions (40, 41). Our findings contribute information relevant to the ongoing debate by showing that the HPC is highly involved during the process of autobiographical memory retrieval [and even more so for the older memories—a finding consistent with our recent report in a separate cohort of patients documenting higher hippocampal sharp ripple rates during retrieval of older autobiographical events (26)]. Hippocampal ripples are widely accepted to be a physiological marker for episodic memory processing (42). Hence, the ability of patients with hippocampal (HPC) lesions to retrieve older memories should not be taken to imply that, in normal human brains, the HPC is not implicated in such functions.

Our findings endorse a dynamic theoretical model which posits memory retrieval in noncompromised individuals involves a temporally well-orchestrated cascade of events that begins with hippocampal LF activity (including the well-known theta range) which, in turn, recruits a large mantle of the midline cortical and anterior thalamic sites. Our results demonstrate that in the process of retrieval, increased LF activity in the HPC precedes network-wide cross-regional phase coherence while HPC stimulation results in a network-wide coherence of the LF activity across the sites (i.e., ITPC & ISPC). Locking of LF-phase (including phase of theta band) reflects synchronization of the timing of neuronal assemblies that fire together (27, 43–48). Therefore, our findings highlight an important role for the HPC as a "universal synchronizer" enabling cross-regional interplay and binding across multiple brain regions. As such, the HPC can be seen as a mnemonic "hub" coordinating the engagement of other regions by phase resetting and creating cross-regional phase coherence which synchronizes their coengagement in the service of retrieving episodic events. This hypothesis coheres with claims that recall represents a reactivation of multiple traces of memory which are consolidated as "engrams" in sites across the brain (49–51).

As noted, during the retrieval stage, the LF activity in the HPC (i.e., "the glue signal") led to a near-simultaneous increase of the HF power in the HPC and PMC—consistent with our previous observation that HF power in the PMC increases simultaneously with elevated rates of sharp ripples in the HPC (26)—a well-known physiological measure of memory processing [consolidation and reactivation (52–55)]. HF power reflects increases in average firing rates and synaptic exchange (9). We believe the exchange between the HPC and PMC might reflect a process of scene construction (56, 57) and the search or representation of the spatiotemporal contextual information associated with previous memory experience (58–61). In keeping with this, PMC engagement was stronger during retrieval of the most recent compared to relatively older memories or semantic facts.

The finding of simultaneous engagement of the HPC and PMC was validated by the finding of strong causal effective connectivity between the two structures (with HPC→ PMC direction outweighing the PMC → HPC direction, Fig. 5 *A* and *E*). A direct relationship between the HPC and PMC defines a pathway beyond the known Papez circuit—an assertion that has been validated by anatomical tracing studies in the primate brain which document strong direct connections between the MTL and PMC (62). In fact, about half of HPC projections to the mammillary bodies in the rodent brain send direct collateral projections to the PMC (63). Our finding of HPC–PMC dialogue is also consistent with our previous study where we reported a strong electrophysiological coupling (phase-locking) between the entorhinal cortex and ipsilateral retrosplenial cortex in subjects with simultaneous coverage in the two structures using subdural strip electrodes (64). Our findings also lend support to a recent MEG study, in which inhibitory stimulation of the human PMC led to a network-level alteration of MTL-driven oscillatory coupling with the PMC itself and with other posterior cortical structures (65).

Lateral parietal regions (and by extension PMC) could also be hypothesized to function as an "episodic buffer," (66) enabling conscious access to representations of prior experiences (67, 68) in order to guide memory decisions based on the strength of mnemonic evidence (69–71). Our findings of stronger PMC engagement during the retrieval of recent memories (supposedly with stronger mnemonic evidence) support this notion. However, according to the mnemonic buffer hypothesis, the parietal engagement should be generalized across episodic and semantic domains—which is inconsistent with our finding of significantly different and weaker engagement of the PMC during the semantic (Fact) condition (Fig. 3 *C* and *D*).

***Thalamus as the ignitor of autobiographical memory retrieval?*** Our simultaneous recordings in the ANT and other brain regions with intracranial electrodes offer insights into the workings of a so-called "lower subcortical region in a higher brain function" (72). Our data show that following a global intersite coherence of the LF phase, the ANT was the first to show HF activity, which may suggest that the ANT plays a key role in "igniting" the transition to memory processing by facilitating the coactivations of multiple brain regions together (Fig. 4)—but after the LF activity in the HPC has reset the time of activity of these structures. This conclusion is rooted in multiple lines of evidence from our observations: The ANT displayed trial-specific HF modulation suggesting that the memory content changed the mode of its engagement; the ANT showed ISPC with multiple regions following the presentation of the retrieval cue; HF activity in the ANT was captured before the rise of HF power in the HPC; the ANT appeared as a "universal receiver" of information from all other AM-activated sites and, in fact, was the first to show an evoked peak following electrical stimulation of any other region [i.e., when a region X was stimulated, the temporal order of captured evoked responses were Region 1 →ANT, followed by ANT→ Region 2, and then Region 1 → Region 2]. Moreover, the ANT was most likely to synchronize with stimulated sites in the HPC, PMC, and OFC.

Our results resonate well with prior studies of the ANT in the context of memory processing. For instance, during rest and sleep, stimulations of the ANT affect the HPC as well as cortical gamma activity (73); thalamic spindles facilitate cortico-cortical and hippocampo-cortical coripplings (54); thalamic spindles are generated during sleep between cortical down and up-states (74, 75); and finally, sleep spindles precede their neocortical counterparts and were initiated during early phases of thalamic slow oscillations (~1 Hz) (76). Moreover, intracranial recordings from the ANT—coupled with scalp (and but intracranial) EEG in human subjects have shown that higher memory for complex photographic scenes was associated with theta phase synchrony as well as coupling between phase of theta oscillations recorded on the scalp and the power of gamma activity recorded directly from the ANT during encoding of stimuli (77, 78).

The role of the ANT as a key player within the memory system is supported by observations in patients with ANT lesions who are known to suffer from significant deficits in episodic (autobiographical) recollection (79) and disruption of the multiple cognitive domains that are associated with DMN (80). Lesion-symptom mapping, a procedure by which the functional connectivity among regions impacted by a clinical condition is examined, has also revealed a distributed episodic memory circuit which includes the ANT, which is functionally connected with the HPC, PMC, and OFC (81). Studies of deep brain stimulation (DBS) treatment for patients with epilepsy have also shown that in patients who respond to DBS therapy, their ANT regions are more positively correlated to the DMN when compared to nonresponders (82) and one of the prominent side effects associated with ANT DBS is problems with episodic memory (83). In addition, several recent brain mapping studies indicate that the ANT is functionally connected to the cortical nodes of the DMN (80, 84, 85) using the seed-based correlation method or independent component analysis on resting-state imaging data. A previous study Li (19) provided further support for these findings using a tensor-based method where their high-resolution subcortical DMN functional connectivity map illustrated that the ANT displayed greater functional connectivity with the DMN than other thalamic nuclei.

Taken together, the ANT appears to be a key player in memory-based cognitive processes, not simply a relay station for the HPC output (16, 86). Our results are compatible with the notion that the ANT acts as a gatekeeper in the memory system (17, 87). Their location within the thalamus allows them to effectively receive and integrate information from various sources (88). When we stimulated a given region, the ANT was consistently the most likely to synchronize their activity with the stimulated region (Fig. 5) and the first to respond to the stimulation (*SI Appendix*, Table S12). This further emphasizes the active role of the ANT in coordinating and integrating neuronal activity across the brain (84).

Our timing results further suggest that, following this integration process, the ANT "opens the gate" to the HF cascade that occurs during AM processing. However, we are mindful that the specific role of the ANT may vary depending on context, suggesting that more research is required to fully understand the ANT's involvement in memory processes. For instance, it is possible, and even likely, that the ANT HF activity was itself triggered and facilitated by incoming signals from other areas of the brain sending a "top–down" context-dependent signals during recall (such as the prefrontal cortex, PFC, etc.; i.e., regions outside the memory network that were outside the scope our current investigations) (89, 90).

***Orbital and ventromedial PFC in autobiographical memory retrieval.*** In the field of memory research, the OFC has been investigated far less using imaging methods compared with HPC and MTL structures because its location causes significant signal dropout when analyzed with traditional pipelines (1). Therefore, our findings from the OFC offer direct evidence, on an unprecedented timescale, of its functional and intrinsic causal interactions with other structures such as the HPC, PMC, and ANT.

A number of theories have posited that the active maintenance of contextual information in medial PFC provides a "top–down" bias signal that influences behavioral responses. Medial PFC-mediated schemas have been hypothesized to make contextual information available for selecting appropriate actions (91–98). However, we emphasize that the majority of these observations (especially in nonhuman mammals) have been from the dorsomedial PFC, including the anterior cingulate areas. The significantly delayed timing of OFC HF engagement (after ANT, HPC, and PMC) suggests that the OFC may be involved less in setting the schema for recall than in evaluative and integrative functions vital to memory-based decision-making processes.

Our findings, however, support the extant evidence from imaging studies which suggest a strong involvement of the vmPFC region in self-referential processing (11, 12, 99–104). The vmPFC has been shown to play a critical role in internally and self-directed cognitive processes such as memory consolidation, mentalizing about the thoughts and feelings of others, emotional control, empathic decision-making (105), and social cognitive functioning (11, 12, 65, 95, 100, 102–104, 106–115). Moreover, MEG studies have highlighted the importance of ventromedial PFC in facilitating hippocampal activity during self-episodic memory retrieval (116). Neuroimaging data further support the involvement of the mPFC in mood-congruent self-episodic recall (96, 117), retrieval of affective responses to stimuli (118) as well as attribution of affective value to retrieved episodes (119); indeed, mPFC activation has been found to be correlated with the personal significance of the retrieved autobiographical memories (120). Finally, lesion studies have shown that mPFC damage can lead to confabulation (false recollections of personal past experiences) (121) as well as reduced self-awareness and self-reflection (106, 122).

**Limitations and Future Directions.** Our study has several important limitations. First, we focused only on four regions primarily because of lack of sufficient coverage in other regions as the sites of recordings had been motivated by the clinical needs. We acknowledge that autobiographical processing involves additional regions beyond the four regions studied here. For instance, the angular gyrus is another key region of interest (15, 123–125), where we have previously reported (7) similar activations during autobiographical processing. Second, we treated the regions as if each region is a unitary functional unit. Different populations of neurons within the anatomical boundaries of a given structure may play very different functional roles. We have already documented the remarkable heterogeneity of responses within the boundaries of the PMC (126) and others have recently suggested several subdivisions within the PMC (127). Additionally, we grouped the posterior and anterior HPC together while our own recent observations have revealed autobiographical memory-related ripples appearing clearly stronger in the anterior than posterior HPC (26). Prior work has also claimed differential activity along the anterior–posterior axis of the structure (128). A potential avenue of future research would be to compare timing and connectivity analyses across different populations of a given region. Finally, as we have noted, the process of autobiographical memory processing–instead of being a pure memory process—blends several kinds of self-referential constructive processes (25, 38). As such, one may not expect autobiographical memory experimental paradigms to probe episode-specific and memory-pure processes as other lab-based experiments do. However, these statements should not be taken to imply that the electrophysiological responses reported in

our work are not related to autobiographical memory processing as they clearly tracked with the subject's behavior in several ways such as hit trials eliciting significantly higher physiological responses than nonautobiographical fact statements or correct rejection AM trials (Fig. 3). Moreover, inferential reasoning and imagination processes occur also during correct rejections. Yet, we showed statistically stronger HF responses during hits vs. correct rejections. Future studies are needed to explore the causal and differential contribution of each of the regions (and their subregions) in different aspects of self-referential processing.

## Methods

For more details, please see *SI Appendix, Supplementary Material*. In brief, we recruited 31 subjects (age range: 19 to 52 y old, 16 female, *SI Appendix*, Table S1) with focal refractory epilepsy who were implanted with stereotactic electrodes (sEEG, AdTech) to localize their seizure onset zone. Compared to neuroimaging studies, clinical invasive recordings in humans have clear limitations in terms of the small number of recruited subjects and sparse coverage across the brain within each individual. We sought to overcome the sparsity of the sEEG method by aggregating data across a cohort of patients. All the participants had at least one electrode site placed over at least two of the regions surrounding the HPC, PMC, OFC, and/or the anterior nuclei of the thalamus (ANT).

Moreover, the locations of electrodes in each participant were decided purely by clinical evaluation since the invasive procedure of intracranial EEG was primarily conducted for presurgical clinical purposes. As our data were recorded in subjects suffering from epilepsy, this may be seen as a limitation. We note, however, that there is strong evidence documenting that nonlesional epileptic tissue exhibits normal physiological responses to incoming relevant stimuli, which are "seized" or diminished only at the time of an ongoing epileptic pathological activity (129, 130). Given the number of trials in each condition, we believe that only a minority of trials were presented during epileptic discharges. Moreover, in each patient with implanted electrodes, only a minority of electrodes (<20%) show epileptic activity, while the majority of electrodes show no signs of epileptic discharges (9). To mitigate the confounding effects of epilepsy and seizures, we recruited patients with focal seizures who do not have a diffuse brain disease and conducted our experiments outside the window of seizures. Moreover, we reviewed the EEG tracings of the patient with the clinical team prior to testing and made sure that the patient did not have subclinical or clinical seizures prior to testing.

Each subject was monitored in the hospital for approximately 6 to 10 d after the implantation surgery. The Institutional Review Board of Stanford University approved the experiments, and all subjects provided verbal and written informed consent before experiments. All 31 participants completed the Seq Task, and 27 participants completed the Sim Task (tasks described in Fig. 1).

**Data, Materials, and Software Availability.** The code used to derive the connectivity index is available here: https://github.com/JRStieger/ConnectivityIndex/ (131). Materials, data, and associated protocols, including code and scripts, are available to readers. All other data are included in the manuscript and/or *SI Appendix*.


1. B. T. Yeo *et al.*, The organization of the human cerebral cortex estimated by intrinsic functional connectivity. *J. Neurophysiol.* **106**, 1125–1165 (2011).
2. B. J. He, A. Z. Snyder, J. M. Zempel, M. D. Smyth, M. E. Raichle, Electrophysiological correlates of the brain's intrinsic large-scale functional architecture. *Proc. Natl. Acad. Sci. U.S.A.* **105**, 16039–16044 (2008).
3. R. Mukamel *et al.*, Coupling between neuronal firing, field potentials, and FMRI in human auditory cortex. *Science* **309**, 951–954 (2005).
4. Y. Nir *et al.*, Interhemispheric correlations of slow spontaneous neuronal fluctuations revealed in human sensory cortex. *Nat. Neurosci.* **11**, 1100–1108 (2008).
5. M. Dastjerdi *et al.*, Differential electrophysiological response during rest, self-referential, and non-self-referential tasks in human posteromedial cortex. *Proc. Natl. Acad. Sci. U.S.A.* **108**, 3023–3028 (2011).
6. A. Kucyi *et al.*, Intracranial electrophysiology reveals reproducible intrinsic functional connectivity within human brain networks. *J. Neurosci.* **38**, 4230–4242 (2018).
7. B. L. Foster, V. Rangarajan, W. R. Shirer, J. Parvizi, Intrinsic and task-dependent coupling of neuronal population activity in human parietal cortex. *Neuron* **86**, 578–590 (2015).
8. A. Mitra *et al.*, Spontaneous infra-slow brain activity has unique spatiotemporal dynamics and laminar structure. *Neuron* **98**, 297–305.e6 (2018).
9. J. Parvizi, S. Kastner, Promises and limitations of human intracranial electroencephalography. *Nat. Neurosci.* **21**, 474–483 (2018).
10. T. Q. Wu *et al.*, Multisite thalamic recordings to characterize seizure propagation in the human brain. *Brain* **146**, 2792–2802 (2023).
11. D. L. Schacter, D. R. Addis, R. L. Buckner, Remembering the past to imagine the future: The prospective brain. *Nat. Rev. Neurosci.* **8**, 657–661 (2007).
12. R. L. Buckner, J. R. Andrews-Hanna, D. L. Schacter, The brain's default network: Anatomy, function, and relevance to disease. *Ann. N. Y. Acad. Sci.* **1124**, 1–38 (2008).
13. E. A. Maguire, Neuroimaging studies of autobiographical event memory. *Philos. Trans. R. Soc. Lond. B Biol. Sci.* **356**, 1441–1451 (2001).
14. R. N. Spreng, R. A. Mar, A. S. Kim, The common neural basis of autobiographical memory, prospection, navigation, theory of mind, and the default mode: A quantitative meta-analysis. *J. Cogn. Neurosci.* **21**, 489–510 (2009).
15. S. Shepardson, K. Dahlgren, S. Hamann, Neural correlates of autobiographical memory retrieval: An SDM neuroimaging meta-analysis. *Cortex* **166**, 59–79 (2023).
16. J. P. Aggleton, S. M. O'Mara, The anterior thalamic nuclei: Core components of a tripartite episodic memory system. *Nat. Rev. Neurosci.* **23**, 505–516 (2022), 10.1038/s41583-022-00591-8.
17. J. M. Shine, L. D. Lewis, D. D. Garrett, K. Hwang, The impact of the human thalamus on brain-wide information processing. *Nat. Rev. Neurosci.* **24**, 416–430 (2023), 10.1038/s41583-023-00701-0.
18. M. Moscovitch, "Confabulation and the frontal systems: Strategic versus associative retrieval in neuropsychological theories of memory" in *Varieties of Memory and Consciousness: Essays in Honor of Endel Tulving*, H. L. Roediger, F. I. Craik, Eds. (Lawrence Erlbaum Associates, Hillsdale, NJ, 1989), pp. 133–160.
19. J. Li *et al.*, Mapping the subcortical connectivity of the human default mode network. *Neuroimage* **245**, 118758 (2021).
20. M. Girn, R. Setton, G. R. Turner, R. N. Spreng, The "limbic network", comprising orbitofrontal and anterior temporal cortex, is part of an extended default network: Evidence from multi-echo fMRI. *Netw. Neurosci.*, 10.1162/netn_a_00385 (2024).
21. T. Q. Wu *et al.*, Multisite thalamic recordings to characterize seizure propagation in the human brain. *Brain* **146**, 2792–2802 (2023), 10.1093/brain/awad121.
22. J. F. Burke *et al.*, Theta and high-frequency activity mark spontaneous recall of episodic memories. *J. Neurosci.* **34**, 11355–11365 (2014).
23. J. Jacobs, M. J. Kahana, A. D. Ekstrom, I. Fried, Brain oscillations control timing of single-neuron activity in humans. *J. Neurosci.* **27**, 3839–3844 (2007).
24. M. C. Fellner *et al.*, Spectral fingerprints or spectral tilt? Evidence for distinct oscillatory signatures of memory formation. *PLoS Biol.* **17**, e3000403 (2019).
25. M. A. Conway, Memory and the self. *J. Mem. Lang.* **53**, 594–628 (2005).
26. Y. Norman, O. Raccah, S. Liu, J. Parvizi, R. Malach, Hippocampal ripples and their coordinated dialogue with the default mode network during recent and remote recollection. *Neuron* **109**, 2767–2780.e5 (2021).
27. G. Buzsaki, *Rhythms of the Brain* (Oxford University Press, 2006).
28. T. Donoghue *et al.*, Parameterizing neural power spectra into periodic and aperiodic components. *Nat. Neurosci.* **23**, 1655–1665 (2020).
29. S. Makeig *et al.*, Dynamic brain sources of visual evoked responses. *Science* **295**, 690–694 (2002).
30. J. Fell *et al.*, Neural bases of cognitive ERPs: More than phase reset. *J. Cogn. Neurosci.* **16**, 1595–1604 (2004).
31. F. Lopes da Silva, "Event-related potentials: Methodology and quantification" in *Electroencephalography: Basic Principles, Clinical Applications, and Related Fields*, E. Niedermeyer, F. Lopes da Silva, Eds. (Williams & Wilkins, Baltimore, 1993).
32. R. Matsumoto *et al.*, Functional connectivity in the human language system: A cortico-cortical evoked potential study. *Brain* **127**, 2316–2330 (2004).
33. J. M. Shine *et al.*, Distinct patterns of temporal and directional connectivity among intrinsic networks in the human brain. *J. Neurosci.* **37**, 9667–9674 (2017).
34. M. J. Veit *et al.*, Temporal order of signal propagation within and across intrinsic brain networks. *Proc. Natl. Acad. Sci. U.S.A.* **118**, e2105031118 (2021).
35. C. J. Keller *et al.*, Mapping human brain networks with cortico-cortical evoked potentials. *Philos. Trans. R. Soc. Lond. B Biol. Sci.* **369**, 20130528 (2014).
36. B. S. Katerman, Y. Li, J. K. Pazdera, C. Keane, M. J. Kahana, EEG biomarkers of free recall. *Neuroimage* **246**, 118748 (2022).
37. S. H. Siddiqi, K. P. Kording, J. Parvizi, M. D. Fox, Causal mapping of human brain function. *Nat. Rev. Neurosci.* **23**, 361–375 (2022), 10.1038/s41583-022-00583-8.
38. M. A. Conway, C. W. Pleydell-Pearce, The construction of autobiographical memories in the self-memory system. *Psychol. Rev.* **107**, 261–288 (2000).
39. M. Moscovitch, Memory and working-with-memory: A component process model based on modules and central systems. *J. Cogn. Neurosci.* **4**, 257–267 (1992).
40. B. Milner, L. R. Squire, E. R. Kandel, Cognitive neuroscience and the study of memory [Review] [173 refs]. *Neuron* **20**, 445–468 (1998).
41. W. B. Scoville, B. Milner, Loss of recent memory after bilateral hippocampal lesions. *J. Neurol. Neurosurg. Psychiatry* **20**, 11 (1957).
42. G. Buzsaki, Hippocampal sharp wave-ripple: A cognitive biomarker for episodic memory and planning. *Hippocampus* **25**, 1073–1188 (2015).
43. T. Elbert, B. Rockstroh, Threshold regulation—A key to the understanding of the combined dynamics of EEG and event-related potentials. *J. Psychophysiol.* **1**, 317–333 (1987).
44. F. Frohlich, D. A. McCormick, Endogenous electric fields may guide neocortical network activity. *Neuron* **67**, 129–143 (2010).
45. O. Jensen, J. E. Lisman, Hippocampal sequence-encoding driven by a cortical multi-item working memory buffer. *Trends Neurosci.* **28**, 67–72 (2005).
46. J. Fell, N. Axmacher, The role of phase synchronization in memory processes. *Nat. Rev. Neurosci.* **12**, 105–118 (2011).
47. J. Lisman, G. Buzsaki, A neural coding scheme formed by the combined function of gamma and theta oscillations. *Schizophr. Bull.* **34**, 974–980 (2008).
48. J. E. Lisman, O. Jensen, The theta-gamma neural code. *Neuron* **77**, 1002–1016 (2013).
49. T. J. Teyler, P. DiScenna, The hippocampal memory indexing theory. *Behav. Neurosci.* **100**, 147–154 (1986).
50. P. W. Frankland, B. Bontempi, The organization of recent and remote memories. *Nat. Rev. Neurosci.* **6**, 119–130 (2005).

51. J. L. McClelland, B. L. McNaughton, R. C. O'Reilly, Why there are complementary learning systems in the hippocampus and neocortex: Insights from the successes and failures of connectionist models of learning and memory. *Psychol. Rev.* **102**, 419–457 (1995).
52. J. J. Chrobak, G. Buzsaki, High-frequency oscillations in the output networks of the hippocampal-entorhinal axis of the freely behaving rat. *J. Neurosci.* **16**, 3056–3066 (1996).
53. D. Sullivan *et al.*, Relationships between hippocampal sharp waves, ripples, and fast gamma oscillation: Influence of dentate and entorhinal cortical activity. *J. Neurosci.* **31**, 8605–8616 (2011).
54. C. W. Dickey *et al.*, Widespread ripples synchronize human cortical activity during sleep, waking, and memory recall. *Proc. Natl. Acad. Sci. U.S.A.* **119**, e2107797119 (2022).
55. G. Girardeau, M. Zugaro, Hippocampal ripples and memory consolidation. *Curr. Opin. Neurobiol.* **21**, 452–459 (2011).
56. E. A. Maguire, The retrosplenial contribution to human navigation: A review of lesion and neuroimaging findings. *Scand. J. Psychol.* **42**, 225–238 (2001).
57. D. Hassabis, E. A. Maguire, Deconstructing episodic memory with construction. *Trends Cogn. Sci.* **11**, 299–306 (2007).
58. C. Ranganath, M. Ritchey, Two cortical systems for memory-guided behaviour. *Nat. Rev. Neurosci.* **13**, 713–726 (2012).
59. S. Brodt, J. Born, Ripples for recall: The hippocampus constructing the context? *Neuron* **109**, 2646–2648 (2021).
60. G. Buzsaki, E. I. Moser, Memory, navigation and theta rhythm in the hippocampal-entorhinal system. *Nat. Neurosci.* **16**, 130–138 (2013).
61. A. P. Yonelinas, C. Ranganath, A. D. Ekstrom, B. J. Wiltgen, A contextual binding theory of episodic memory: Systems consolidation reconsidered. *Nat. Rev. Neurosci.* **20**, 364–375 (2019).
62. J. Parvizi, G. W. Van Hoesen, J. Buckwalter, A. Damasio, Neural connections of the posteromedial cortex in the macaque. *Proc. Natl. Acad. Sci. U.S.A.* **103**, 1563–1568 (2006).
63. L. Kinnavane, S. D. Vann, A. J. D. Nelson, S. M. O'Mara, J. P. Aggleton, Collateral projections innervate the mammillary bodies and retrosplenial cortex: A new category of hippocampal cells. *eNeuro* **5** (2018).
64. B. L. Foster, A. Kaveh, M. Dastjerdi, K. J. Miller, J. Parvizi, Human retrosplenial cortex displays transient theta phase locking with medial temporal cortex prior to activation during autobiographical memory retrieval. *J. Neurosci.* **33**, 10439–10446 (2013).
65. M. Hebscher, J. A. Meltzer, A. Gilboa, A causal role for the precuneus in network-wide theta and gamma oscillatory activity during complex memory retrieval. *Elife* **8**, e43114 (2019).
66. A. Baddeley, The episodic buffer: A new component of working memory? *Trends Cogn. Sci.* **4**, 417–423 (2000).
67. K. L. Vilberg, M. D. Rugg, Memory retrieval and the parietal cortex: A review of evidence from a dual-process perspective. *Neuropsychologia* **46**, 1787–1799 (2008).
68. M. D. Rugg, K. L. Vilberg, Brain networks underlying episodic memory retrieval. *Curr. Opin. Neurobiol.* **23**, 255–260 (2013).
69. A. D. Wagner, B. J. Shannon, I. Kahn, R. L. Buckner, Parietal lobe contributions to episodic memory retrieval. *Trends Cogn. Sci.* **9**, 445–453 (2005).
70. J. Parvizi, A. D. Wagner, Memory, numbers, and action decision in human posterior parietal cortex. *Neuron* **97**, 7–10 (2018).
71. A. Gonzalez *et al.*, Electrocorticography reveals the temporal dynamics of posterior parietal cortical activity during recognition memory decisions. *Proc. Natl. Acad. Sci. U.S.A.* **112**, 11066–11071 (2015).
72. J. Parvizi, Corticocentric myopia: Old bias in new cognitive sciences. *Trends Cogn. Sci.* **13**, 354–359 (2009).
73. G. Chaitanya *et al.*, Precision mapping of the epileptogenic network with low- and high-frequency stimulation of anterior nucleus of thalamus. *Clin. Neurophysiol.* **131**, 2158–2167 (2020).
74. R. A. Mak-McCully *et al.*, Coordination of cortical and thalamic activity during non-REM sleep in humans. *Nat. Commun.* **8**, 15499 (2017).
75. C. E. Gonzalez *et al.*, Theta bursts precede, and spindles follow, cortical and thalamic downstates in human NREM sleep. *J. Neurosci.* **38**, 9989–10001 (2018).
76. T. Schreiner, E. Kaufmann, S. Noachtar, J. H. Mehrkens, T. Staudigl, The human thalamus orchestrates neocortical oscillations during NREM sleep. *Nat. Commun.* **13**, 5231 (2022).
77. C. M. Sweeney-Reed *et al.*, Corticothalamic phase synchrony and cross-frequency coupling predict human memory formation. *Elife* **3**, e05352 (2014).
78. C. M. Sweeney-Reed *et al.*, Thalamic theta phase alignment predicts human memory formation and anterior thalamic cross-frequency coupling. *Elife* **4**, e07578 (2015).
79. N. D. Child, E. E. Benarroch, Anterior nucleus of the thalamus: Functional organization and clinical implications. *Neurology* **81**, 1869–1876 (2013).
80. D. T. Jones, F. J. Mateen, C. F. Lucchinetti, C. R. Jack Jr., K. M. Welker, Default mode network disruption secondary to a lesion in the anterior thalamus. *Arch Neurol.* **68**, 242–247 (2011).
81. M. A. Ferguson *et al.*, A human memory circuit derived from brain lesions causing amnesia. *Nat. Commun.* **10**, 3497 (2019).
82. E. H. Middlebrooks *et al.*, Differences in functional connectivity profiles as a predictor of response to anterior thalamic nucleus deep brain stimulation for epilepsy: A hypothesis for the mechanism of action and a potential biomarker for outcomes. *Neurosurg. Focus* **45**, E7 (2018).
83. R. Fisher *et al.*, Electrical stimulation of the anterior nucleus of thalamus for treatment of refractory epilepsy. *Epilepsia* **51**, 899–908 (2010).
84. C. M. Sweeney-Reed *et al.*, The role of the anterior nuclei of the thalamus in human memory processing. *Neurosci. Biobehav. Rev.* **126**, 146–158 (2021).
85. P. N. Alves *et al.*, An improved neuroanatomical model of the default-mode network reconciles previous neuroimaging and neuropathological findings. *Commun. Biol.* **2**, 370 (2019).
86. P. T. Bell, J. M. Shine, Subcortical contributions to large-scale network communication. *Neurosci. Biobehav. Rev.* **71**, 313–322 (2016).
87. A. C. Toader *et al.*, Anteromedial thalamus gates the selection and stabilization of long-term memories. *Cell* **186**, 1369–1381.e17 (2023).
88. K. Hwang, M. A. Bertolero, W. B. Liu, M. D'Esposito, The human thalamus is an integrative hub for functional brain networks. *J. Neurosci.* **37**, 5594–5607 (2017).
89. P. Rajasethupathy *et al.*, Projections from neocortex mediate top-down control of memory retrieval. *Nature* **526**, 653–659 (2015).
90. Z. V. Guo *et al.*, Maintenance of persistent activity in a frontal thalamocortical loop. *Nature* **545**, 181–186 (2017).
91. A. Gilboa, M. Moscovitch, Ventromedial prefrontal cortex generates pre-stimulus theta coherence desynchronization: A schema instantiation hypothesis. *Cortex* **87**, 16–30 (2017).
92. W. H. Alexander, J. W. Brown, Medial prefrontal cortex as an action-outcome predictor. *Nat. Neurosci.* **14**, 1338–1344 (2011).
93. E. K. Miller, J. D. Cohen, An integrative theory of prefrontal cortex function. *Annu. Rev. Neurosci.* **24**, 167–202 (2001).
94. V. E. Ghosh, M. Moscovitch, B. Melo Colella, A. Gilboa, Schema representation in patients with ventromedial PFC lesions. *J. Neurosci.* **34**, 12057–12070 (2014).
95. M. Hebscher, A. Gilboa, A boost of confidence: The role of the ventromedial prefrontal cortex in memory, decision-making, and schemas. *Neuropsychologia* **90**, 46–58 (2016).
96. A. R. Preston, H. Eichenbaum, Interplay of hippocampus and prefrontal cortex in memory. *Curr. Biol.* **23**, R764–R773 (2013).
97. D. R. Euston, A. J. Gruber, B. L. McNaughton, The role of medial prefrontal cortex in memory and decision making. *Neuron* **76**, 1057–1070 (2012).
98. A. Bechara, H. Damasio, A. R. Damasio, Emotion, decision making and the orbitofrontal cortex [Review] [62 refs]. *Cereb. Cortex* **10**, 295–307 (2000).
99. J. S. Beer, M. V. Lombardo, J. P. Bhanji, Roles of medial prefrontal cortex and orbitofrontal cortex in self-evaluation. *J. Cogn. Neurosci.* **22**, 2108–2119 (2010).
100. G. Northoff *et al.*, Self-referential processing in our brain–A meta-analysis of imaging studies on the self. *Neuroimage* **31**, 440–457 (2006).
101. C. L. Philippi, M. C. Duff, N. L. Denburg, D. Tranel, D. Rudrauf, Medial PFC damage abolishes the self-reference effect. *J. Cogn. Neurosci.* **24**, 475–481 (2012).
102. M. Koenigs *et al.*, Damage to the prefrontal cortex increases utilitarian moral judgements. *Nature* **446**, 908–911 (2007).
103. F. De Brigard, R. Nathan Spreng, J. P. Mitchell, D. L. Schacter, Neural activity associated with self, other, and object-based counterfactual thinking. *Neuroimage* **109**, 12–26 (2015).
104. A. Gilboa, G. Winocur, C. L. Grady, S. J. Hevenor, M. Moscovitch, Remembering our past: Functional neuroanatomy of recollection of recent and very remote personal events. *Cereb. Cortex* **14**, 1214–1225 (2004).
105. V. Janowski, C. Camerer, A. Rangel, Empathic choice involves vmPFC value signals that are modulated by social processing implemented in IPL. *Soc. Cogn. Affect. Neurosci.* **8**, 201–208 (2013).
106. C. L. Philippi, M. C. Duff, N. L. Denburg, D. Tranel, D. Rudrauf, Medial PFC damage abolishes the self-reference effect. *J. Cogn. Neurosci.* **24**, 475–481 (2012).
107. R. N. Spreng *et al.*, The default network of the human brain is associated with perceived social isolation. *Nat. Commun.* **11**, 6393 (2020).
108. L. Mwilambwe-Tshilobo, R. Setton, D. Bzdok, G. R. Turner, R. N. Spreng, Age differences in functional brain networks associated with loneliness and empathy. *Netw Neurosci.* **7**, 496–521 (2023).
109. L. Mwilambwe-Tshilobo, R. N. Spreng, Social exclusion reliably engages the default network: A meta-analysis of Cyberball. *Neuroimage* **227**, 117666 (2021).
110. E. DuPre, R. N. Spreng, Structural covariance networks across the life span, from 6 to 94 years of age. *Netw. Neurosci.* **1**, 302–323 (2017).
111. A. C. Laurita, E. DuPre, N. C. Ebner, G. R. Turner, R. N. Spreng, Default network interactivity during mentalizing about known others is modulated by age and social closeness. *Soc. Cogn. Affect. Neurosci.* **15**, 537–549 (2020).
112. A. C. Laurita, C. Hazan, R. N. Spreng, An attachment theoretical perspective for the neural representation of close others. *Soc. Cogn. Affect. Neurosci.* **14**, 237–251 (2019).
113. A. C. Laurita, C. Hazan, R. N. Spreng, Dissociable patterns of brain activity for mentalizing about known others: A role for attachment. *Soc. Cogn. Affect. Neurosci.* **12**, 1072–1082 (2017).
114. J. S. Beer, M. V. Lombardo, J. P. Bhanji, Roles of medial prefrontal cortex and orbitofrontal cortex in self-evaluation. *J. Cogn. Neurosci.* **22**, 2108–2119 (2010).
115. M. Levorsen, R. Aoki, K. Matsumoto, C. Sedikides, K. Izuma, The self-concept is represented in the medial prefrontal cortex in terms of self-importance. *J. Neurosci.* **43**, 3675–3686 (2023).
116. C. McCormick, D. N. Barry, A. Jafarian, G. R. Barnes, E. A. Maguire, vmPFC drives hippocampal processing during autobiographical memory recall regardless of remoteness. *Cereb. Cortex* **30**, 5972–5987 (2020).
117. D. A. Fitzgerald *et al.*, How mood challenges emotional memory formation: An fMRI investigation. *Neuroimage* **56**, 1783–1790 (2011).
118. K. C. Berridge, Pleasures of the brain. *Brain Cogn.* **52**, 106–128 (2003).
119. M. L. Kringelbach, E. T. Rolls, The functional neuroanatomy of the human orbitofrontal cortex: Evidence from neuroimaging and neuropsychology. *Prog. Neurobiol.* **72**, 341–372 (2004).
120. W. J. Lin, A. J. Horner, N. Burgess, Ventromedial prefrontal cortex, adding value to autobiographical memories. *Sci. Rep.* **6**, 28630 (2016).
121. A. Gilboa *et al.*, Mechanisms of spontaneous confabulations: A strategic retrieval account. *Brain* **129**, 1399–1414 (2006).
122. M. Koenigs *et al.*, Distinct regions of prefrontal cortex mediate resistance and vulnerability to depression. *J. Neurosci.* **28**, 12341–12348 (2008).
123. M. D. Rugg, D. R. King, Ventral lateral parietal cortex and episodic memory retrieval. *Cortex* **107**, 238–250 (2018).
124. L. Bréchet, P. Grivaz, B. Gauthier, O. Blanke, Common recruitment of angular gyrus in episodic autobiographical memory and bodily self-consciousness. *Front. Behav. Neurosci.* **12**, 270 (2018).
125. C. Sestieri, M. Corbetta, G. L. Romani, G. L. Shulman, Episodic memory retrieval, parietal cortex, and the default mode network: Functional and topographic analyses. *J. Neurosci.* **31**, 4407–4420 (2011).
126. A. L. Daitch, J. Parvizi, Spatial and temporal heterogeneity of neural responses in human posteromedial cortex. *Proc. Natl. Acad. Sci. U.S.A.* **115**, 4785–4790 (2018), 10.1073/pnas.1721714115.
127. B. L. Foster *et al.*, A tripartite view of the posterior cingulate cortex. *Nat. Rev. Neurosci.* **24**, 173–189 (2023).
128. A. Goyal *et al.*, Functionally distinct high and low theta oscillations in the human hippocampus. *Nat. Commun.* **11**, 2469 (2020).
129. S. Akkol *et al.*, Intracranial electroencephalography reveals selective responses to cognitive stimuli in the periventricular heterotopias. *J. Neurosci.* **41**, 3870–3878 (2021).
130. S. Liu, J. Parvizi, Cognitive refractory state caused by spontaneous epileptic high-frequency oscillations in the human brain. *Sci. Transl. Med.* **11**, eaax7830 (2019).
131. J. Stieger, Analysis of Connectivity Index. Github Database. https://github.com/JRStieger/ConnectivityIndex. Deposited 16 July 2024.